Received: 29 November 2020 | Revised: 22 May 2021 | Accepted: 18 August 2021

DOI: 10.1002/prot.26224

RESEARCH ARTICLE

PROTEINS WILEY

How phosphorylation of peptides affects their interaction with 14-3-3η domains

Nicolas Künzel[1,2] | Volkhard Helms[1,2]

[1]Center for Bioinformatics, Saarland University, Saarbrücken, Germany

[2]Center for Bioinformatics, Saarland Informatics Campus, Saarland University, Postfach 15 11 50, 66041, Saarbrücken, Germany

Correspondence
Volkhard Helms, Center for Bioinformatics, Saarland University, Saarbrücken, Germany.
Email: volkhard.helms@bioinformatik.uni-saarland.de

Funding information
Deutsche Forschungsgemeinschaft, Grant/Award Number: He 3875/14-1; Resource for Biocomputing, Visualization, and Informatics at the University of California, San Francisco, with support from NIH, Grant/Award Number: P41-GM103311; Universitaet des Saarlandes (Projekt DEAL)

Abstract

Members of the 14-3-3 domain family have important functions as adapter domains. Via an amphipathic groove on their protein surface they typically bind to disordered C-terminals of other proteins. Importantly, binding partners of 14-3-3 domains usually contain a phosphorylated serine or threonine residue at their binding interface and possess one of three different sequence motifs. Binding of the respective unphosphorylated versions of the peptides is typically strongly disfavored. There is a wealth of structural and thermodynamic data available for the phosphorylated forms but not for the unphosphorylated forms as the binding affinities seem to be too weak to be measurable experimentally. Here, we characterized the mechanistic details that govern the preference for the binding of phosphorylated peptides to 14-3-3η domains by means of molecular dynamics (MD) simulations. We found that the phosphate group is ideally coordinated in the binding pocket whereas the respective unphosphorylated side-chain counterpart is not. Thus, the binding preference results from the tight coordination of the phosphorylated residue at the center of the binding interface. Furthermore, MD simulations of 14-3-3η dimers showed a preference for the simultaneous binding of two phosphorylated peptides in agreement with their experimentally observed cooperativity.

KEYWORDS
free energy calculation, molecular dynamics simulation, peptide–protein complex, post translational modification

1 | INTRODUCTION

The 14-3-3 proteins are a family of adapter proteins performing regulatory functions in cell-cycle control, signal transduction, protein trafficking, and apoptosis. They are abundant in nearly all eukaryotic cells and occur predominantly as stably folded homodimers and heterodimers[1,2] being stabilized by salt bridges and hydrophobic interactions.[3,4] There exist seven known isoforms in human, namely α/β, γ, ε, η, ζ/δ, θ, and σ, exhibiting high sequence and structural similarity (RMS deviations between 0.7 and 1.8 Å).[5] Each monomer is composed of nine α-helices, forming an amphipathic groove that creates the main binding interface between 14-3-3 proteins and their target proteins.[6] In this groove lysine and arginine residues form a basic cluster that mediates the interaction with 14-3-3 binding partners.[6–8]

The 14-3-3 proteins interact with disordered regions of various phosphorylated proteins that most commonly contain motif 1 (R[S/F/Y/W]XpSXP), motif 2 (RX[S/Y/FW/T/Q/A/D]Xp[S/T]X[P/L/M]),[9–11] or motif 3 (RXXp[S/T]XX-COOH)[10] sequences but also with a few unphosphorylated peptides,[6,7,12] such as the exoenzyme S (ExoS)[13] or the carbohydrate-response element-binding protein (ChREBP).[14,15] To

our knowledge there exist hardly any experimental data, such as binding constants, for the unphosphorylated counterparts of phosphorylated motif 1 and motif 2 peptides. The binding of these unphosphorylated peptides seems to be too weak to be measurable[9,16,17] and only a lower barrier for the binding constant K_d for the RSRSTSTP peptide exists.[9] Interestingly, it was shown that 14-3-3 dimers are able to bind simultaneously to two target sequences contained in a single polypeptide chain, that leads to an increase in binding affinity compared with the binding at only one binding site.[9,17–19] This effect has been termed cooperative binding.[9] It was suggested that complexation at the first binding site acts as a gatekeeper necessary for 14-3-3 binding but may not be sufficient in order to enable full biological activity.[18]

The main aim of this study was therefore to mechanistically explain why 14-3-3 proteins preferably bind to phosphorylated peptides. To this aim we studied complexes of 14-3-3η proteins with phosphorylated motif 1 (c-RAF-pS259 (RSRSTpSTP) and c-Raf-pS233 (HRYpSTP)) as well as motif 2 (RLYHpSLP) peptides together with their unphosphorylated counterparts by means of unbiased molecular dynamics (MD) and alchemical transformation simulations in silico.

2 | METHODS

2.1 | Structure preparation

For this study we selected the 14-3-3η domain with various peptides because their binding affinities have been extensively characterized by Yaffe et al.[9] So far, no crystal structures have been reported for the complex of the 14-3-3η domain bound to the c-RAF-1 peptides RSRSTpSTP, RSRSTSTP, HRYpSTP and HRYSTP. Thus, we superimposed an X-ray structure of the 14-3-3ζ dimer in complex with the RSRSTpSTPNV peptide (Protein Data Bank [PDB][20] entry 4FJ3[19]) onto a crystal structure of the 14-3-3η dimer bound to another peptide (PDB entry 2C63[21]) using UCSF Chimera.[22] The overall alignment yielded a low RMSD of 0.98 Å for the corresponding C_α atoms. Also the binding modes of the two peptides were very similar (C_α-RMSD with aligned 14-3-3 dimers: 1.52 Å). We used the coordinates of the superimposed RSRSTpSTPNV and HRYpSTP peptides as starting points for the MD simulations of the 14-3-3η dimers bound to these peptides. When studying complexes with the shorter RSRSTpSTP peptide we simply deleted the last two residues.

The same procedure was applied to obtain starting conformations of 14-3-3η bound to the RLYHpSLP peptide. Here, we used an X-ray structure of a 14-3-3ζ dimer binding this peptide (PDB entry 1QJA[23]) and superimposed it onto the same crystal structure of the 14-3-3η dimer binding to another peptide (PDB entry 2C63[21]) as above. Again, the alignment resulted in a very low C_α-RMSD of 0.835 Å. For all monomer simulations we used the structure of the 14-3-3η monomer binding to the respective ligand taken from the aligned dimer structures.

In order to obtain starting conformations of 14-3-3η bound to the unphosphorylated peptides we removed the phosphate group from the phosphoserine residues using the rotamer replacement function implemented in UCSF Chimera[22] by applying the serine rotamer from the Dunbrack rotamer library.[24] After energy minimization and equilibration, the structure showed only minor deviations (RSRSTSTP C_α-RMSD of 1.47 Å from the RSRSTpSTP structure in the bound state).

For the alchemical free energy simulations, hybrid structures and topologies including the unphosphorylated and phosphorylated residues in the same file were obtained using the tool PMX.[25,26] Since no hybrid structures for phosphorylated serines existed in the published program, these were kindly provided by Dr. V. Gapsys for the CHARMM36m[27] force field.

2.2 | Molecular dynamics simulations

All MD simulations were performed using the GROMACS[28] 2018.8 software package with the CHARMM36m[27] force field for proteins and peptides. Water molecules were represented by the TIP3P[29] model modified for the CHARMM force field.[30] Hydrogen atoms were generated using the internal GROMACS tool pdb2gmx. In the simulations we applied a time step of 2 fs and periodic boundary conditions.[31] Long-range electrostatic interactions were computed with the particle-mesh-Ewald summation method[32] and the nonbonded interaction cutoff was set to 12 Å. All bonds were constrained using the LINCS[33] algorithm (in plain MD simulations only H-bonds were constrained). Long range dispersion corrections were applied for energy and pressure. A concentration of 0.15 mol/L NaCl was included in all simulation boxes in order to mimic physiological conditions.

Initially, the systems were minimized in two steps. First the unsolvated molecular system was minimized using the steepest descent algorithm for a total of 50 000 steps with an initial step size of 0.01 nm and a convergence value for the maximal force of 5 kJ/mol/nm. After solvating and ionizing the system, a minimization was carried out, using the steepest descent algorithm for a total of 100 000 steps with an initial step size of 0.01 nm and a convergence value of 500 kJ/mol/nm. During these steps the positions of the heavy protein and peptide atoms were kept rigid using position restraints.

Afterwards the systems were thermalized for 500 ps each at 100 K, 200 K, and at the final temperature of 298.15 K, respectively, while keeping the position restraints for the proteins and peptides. These steps used the velocity-rescaling thermostat[34] with a coupling time constant of 0.1 ps and a separate temperature bath for solute and solvent. The equilibration was continued for another 500 ps in the NPT ensemble by adding a Berendsen barostat[35] with a time constant of 2.0 ps, a reference pressure of 1 bar, and an isothermal compressibility of 4.6×10^{-5} bar^{-1} while still keeping the position restraints of the solute. Thereafter, the Berendsen barostat[35] was changed to a Parrinello–Rahman extended-ensemble pressure coupling[36,37] because the former one does not yield a correct thermodynamic ensemble, but is very efficient for the scaling of a box during the start of a simulation. The position restraints were released in three steps from 1000 via 100, and 10 to 0 kJ/mol/nm^2.

Subsequently, unbiased production runs were performed. Coordinates were recorded every 10 ps.

2.2.1 | Unbiased MD simulations

For the plain MD simulations a triclinic box was created such that the minimal distance of every solute atom from the edge of the box was at least 1.5 nm. This resulted in a size of 8.5 nm × 7.5 nm × 9.0 nm for the 14-3-3η monomer and 12.0 nm × 8.0 nm × 10.0 nm for the 14-3-3η dimer simulations, respectively.

We simulated two systems in the absence of a peptide: the 14-3-3η monomer and the 14-3-3η dimer, as well as six systems containing a single peptide: the 14-3-3η monomer with the peptides RSRSTpSTP, RSRSTSTP, RLYHpSLP, and RLYHSLP and the 14-3-3η dimer with the peptides RSRSTpSTP and RSRSTSTP. Additionally, we simulated another four dimer systems where each monomer was bound to a peptide: the 14-3-3η dimer with RSRSTpSTP and HRYpSTP, with RSRSTpSTP and HRYSTP, with RSRSTSTP and HRYpSTP and with RSRSTSTP and HRYSTP. Each system was simulated three times for 1 μs each. To compare the results with the free states we also simulated the unbound RSRSTSTP/RSRSTpSTP and RLYHSLP/RLYHpSLP peptides in a water box, each one once for 1 μs.

All together this sums up to a total of 40 μs of simulation time.

2.2.2 | Analysis tools

Hydrogen bonds and contacts were identified in the trajectories using the MDTraj[38] python toolkit using the "Baker-Hubbard"[39] and "compute contacts" algorithms. The number of hydrogen bonds formed by the phosphoserine or serine residues at the relevant positions were computed with the gmx hbond tool. The root mean square fluctuations (RMSFs) were characterized by the gmx rmsf tool and the principal component analysis (PCA) was carried out with the gmx colvar and gmx aneig tools, all included in GROMACS.[28]

2.3 | Alchemical free energy simulations

Alchemical free energy differences were computed by performing repeated non-equilibrium simulations along the reaction path and calculating the free energy difference using two methods based on the Jarzynski equality,[40] namely the Bennett acceptance ratio (BAR)[41] and the Crooks Gaussian Intersection[42] method, respectively.

The four relevant states of each system were the unbound phosphorylated peptide, the unbound unphosphorylated peptide, the bound phosphorylated peptide and the bound unphosphorylated peptide. These can be arranged into the thermodynamic cycle shown in Figure 1. The difference in binding free energy is then obtained from the thermodynamic cycle as

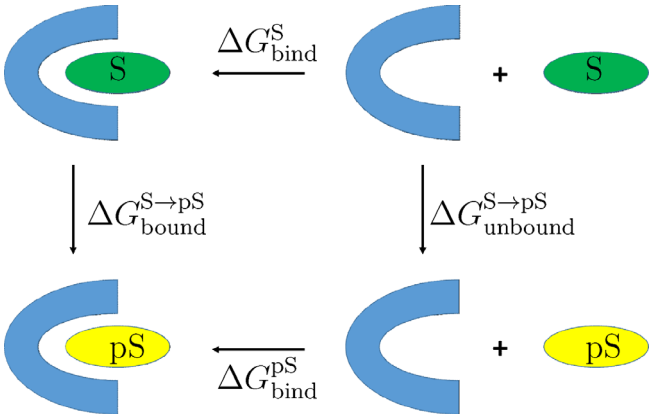

FIGURE 1 Thermodynamic cycle to compute the difference in binding free energy between phosphorylated (denoted pS) and unphosphorylated peptides (on serine, denoted S) complexed in complex with a protein domain (depicted in blue)

$$\Delta\Delta G_{bind} = \Delta G^{pS}_{bind} - \Delta G^{S}_{bind} = \Delta G^{S\to pS}_{bound} - \Delta G^{S\to pS}_{unbound}. \quad (1)$$

The superscript S denotes the unphosphorylated peptide containing a serine while the superscript pS denotes the phosphorylated peptide containing a phosphoserine. These kind of simulations do not allow to calculate absolute free energy values for the binding of a peptide to a protein but yield the difference in binding free energy between two different peptides (here, the phosphorylated and unphosphorylated peptide) binding to the same protein. In free energy perturbation methods the change from one state A to the other state B is typically implemented by using a coupling parameter λ that changes the topology from A to B gradually. During the course of the simulation the work performed on the system is computed and the change in free energy during that process is evaluated using the BAR.[41] In our case the resulting binding free energy difference is calculated as the difference between the two alchemical transformations in the bound and free state (see Equation (1)).

In experiments one usually measures the dissociation constant K_D that is directly related to the binding free energy by

$$\Delta G^{0}_{bind} = -k_B T \ \ln(c_0 K_D), \quad (2)$$

with the Boltzmann constant k_B, temperature T, at the standard concentration $c_0 = 1^{-1} \approx 1/1661\,\text{Å}^{-3}$. Since the transformations of the free and bound peptides are performed in simulation boxes of different, finite sizes resulting in different concentrations of the solute, both transformation free energies have to be corrected for the box size using the standard concentration. The corrected standard binding free energy[43,44] is then

$$\Delta G^{0}_{bind} = \Delta G^{simulation}_{bind} - k_B T \ \ln(c_0 V_{box}) \quad (3)$$

where, V_{box} is the volume of the simulation box.

Introducing a phosphate group during the course of a simulation substantially alters the total charge of the system. This can lead to artifacts in the simulations and thus the calculated free energies have to be corrected.[45–49] An elaborate correction scheme when using lattice-sum methods was derived by Rocklin et al.[49] This method was originally designed for free energy perturbation simulations calculating absolute binding free energies where the bound ligand is alchemically transformed into a non-interacting dummy molecule. In our alchemical transformations the ligand is transformed from one state to another one and thus the correction scheme has to be adapted. Chen et al.[50] derived a correction scheme for relative binding free energies for ligands with different charges, as is the case in our systems. They assumed that the protein charge is zero, thus all terms involving it were left out. We also included the empirical correction term of Rocklin et al.[49] A derivation is shown in the Supporting Information. The resulting corrections terms are

$$\Delta\Delta G^{A\to B}_{\mathrm{NET\_USV,state}}(L_{\mathrm{state}}) = -\frac{\xi_{LS}}{8\pi\varepsilon_0\varepsilon_S}\left[\left(Q_L^B\right)^2 - \left(Q_L^A\right)^2 + 2Q_P\left(Q_L^B - Q_L^A\right)\right]\frac{1}{L_{\mathrm{state}}} \tag{4}$$

for the periodicity–induced net–charge interactions and undersolvation,[49]

$$\Delta\Delta G^{A\to B}_{\mathrm{RIP,state}}(L_{\mathrm{state}}) = \left[\left(I^B_{P,\mathrm{state}} + I^B_{L,\mathrm{state}}\right)Q_L^B - \left(I^A_{P,\mathrm{state}} + I^A_{L,\mathrm{state}}\right)Q_L^A + \left(I^B_{L,\mathrm{state}} - I^A_{L,\mathrm{state}}\right)Q_P\right]\frac{1}{L^3_{\mathrm{state}}} \tag{5}$$

for the residual integrated potential effects,[49]

$$\Delta\Delta G^{A\to B}_{\mathrm{EMP,state}}(L_{\mathrm{state}}) = -\frac{1}{8\pi\varepsilon_0}\frac{16\pi^2}{45}\left(1-\frac{1}{\varepsilon_S}\right) \times\left(\left[\left(Q_P + Q_L^B\right)^2 - Q_P^2\right]\left(R^B_{L,\mathrm{state}}\right)^5 - \left[\left(Q_P + Q_L^A\right)^2 - Q_P^2\right]\left(R^A_{L,\mathrm{state}}\right)^5\right)\frac{1}{L^6_{\mathrm{state}}}$$

as additional empirical correction term[49] with $R^X_{L,\mathrm{state}} = \left(\left[\frac{1}{8\pi\varepsilon_0}\frac{4\pi}{3}\left(1-\frac{1}{\varepsilon_S}\right)Q_L^X\right]^{-1} I^X_{L,SLV,\mathrm{state}}\right)^{1/2}$ and

$$\Delta\Delta G^{A\to B}_{\mathrm{DSC,state}}(L_{\mathrm{state}})(N_S, L) = -\frac{\gamma_S}{6\varepsilon_0}\frac{N_{S,\mathrm{state}}}{L^3_{\mathrm{state}}}\left(Q_L^B - Q_L^A\right) \tag{7}$$

for discrete solvent effects. "X" can be either state "A" or "B," Q_P is the net charge of the protein, Q_L^X denotes the net charge of the ligands, ε_S is the static relative dielectric permittivity of the solvent, $\xi_{LS} \approx -2.837297$ is the cubic lattice-sum (Wigner) integration constant, "state" can be either "bound" or "free," and L_{state} is the size of the simulation box in the respective state.

For the alchemical simulations of a 14-3-3η monomer bound to a peptide and another unbound peptide, a cubic box was created such that the minimal distance of every atom of the solute was at least 1.5 nm from the box edge resulting in a size of around 10.2 nm per edge for the simulations of the bound state and 5.3 nm per edge for the simulations of the free state. The (unbiased) equilibrium simulation lasted 20 ns. The first 4 ns were discarded and 100 starting structures for the alchemical transformations were recorded every 16 snapshots (i.e., every 160 ps). Each of these 100 transformations was performed for 1 ns by gradually changing the parameter λ each step by $\Delta\lambda = 0.2 \cdot 10^{-5}$ from 0 to 1 during the course of the simulation. The change of the Hamiltonian with respect to the coupling parameter λ was saved every time step. We repeated these simulations four to seven times for every system to obtain a statistical error.

To ensure smooth convergence of the derivatives of the non-bonded energy terms while creating or annihilating atoms, we used a soft-core potential with soft-core parameter $\alpha_{SC} = 0.3$, soft-core power $p_{SC} = 1$ and radius of the interaction set to $\sigma_{SC} = 0.25$. The alchemical transformations were performed both in the forward and backward directions, that is, from $\lambda = 0$ to 1 and from $\lambda = 1$ to 0, in order to achieve better convergence. The results were then combined using an analysis tool included in the PMX package,[25] which calculates the free energy difference using the BAR,[41] the Jarzynski equality[40] and the Crooks Gaussian Intersection[42] method. All results shown in this study were obtained using BAR, but results were only considered valid when all three estimators gave similar estimates, which is a good measure for convergence of such non-equilibrium methods.[40,51]

As stated before, the simulations for the transformation of the free and bound peptides were performed in simulation boxes of different, finite sizes resulting in different concentrations of the solute. Thus, the results were corrected for the box size using the standard concentration c_0[44] and likewise for electrostatic finite-size effects.[49]

3 | RESULTS

3.1 | Unbiased MD simulations

MD simulations of 14-3-3η monomers and dimers complexed with either phosphorylated or unphosphorylated peptides or both were stable on the 1 μs time scale studied here. The mean C_α-RMS deviations from (modified) crystal structures are listed in Table 1. The only exceptions to this were a single simulation of 14-3-3η with the RLYHSLP peptide and another simulation of a 14-3-3η dimer with the RSRSTpSTP and HRYSTP peptides bound at the same time. In these simulations unbinding of the unphosphorylated peptides happened. Hence, we repeated the one with RLYSLP and cut the trajectory with RSRSTpSTP and HRYSTP in order to keep only the part of the trajectory without the unbinding event in order to obtain trajectories without unbinding events. Figure 2 shows representative snapshots from the simulations of a 14-3-3η monomer with the RSRSTpSTP and RSRSTSTP peptides. Both peptides remained bound in the binding groove.

The X-ray structure of 14-3-3η bound to RSRSTpSTP and the conformations sampled in the simulations suggest that there exists a strong difference in how tightly phosphorylated and

unphosphorylated peptides are coordinated in the 14-3-3 binding groove. To quantify this, we extracted mean distances between peptide and protein residues from the plain MD simulations. Protein and peptide residues were defined to be in contact when the mean distance between them was below 4 Å over the full simulation length. Overall, the 14-3-3η protein formed a total of 31 relevant contacts with the RSRSTpSTP peptide (four contacts had distances of <2 Å) and 13 relevant contacts with the RSRSTSTP peptide (no contact had a distance shorter than 2 Å; see Table 2).

In particular, both peptides formed very strong interactions between their Pro261 residue and Lys50 and Lys125 of the protein (van-der-Waals contacts and very negative mean interaction energies) even though hydrogen bonds between these residues are only found in around 35%–40% of the frames with the phosphorylated RSRSTpSTP peptide bound and in 65%–70% of the frames with the unphosphorylated RSRSTSTP peptide bound (see Table 4). Similar interactions were observed for the 14-3-3η monomer binding RLYHSLP/RLYHpSLP with hydrogen bonds and contacts between Pro9 of the peptide and Lys50 or Lys125 of the protein and hydrogen-bond occupancies in the same range (see Table S1), as well as for 14-3-3η dimers binding two peptides (RSRSTSTP/RSRSTpSTP + HRYSTP/HRYpSTP) at the same time. For the 14-3-3η dimer complexed with RSRSTpSTP no hydrogen bonds were formed that involve Pro261 whereas the occupancy of the hydrogen bonds for Pro261 for RSRSTSTP was much lower for the dimer than for the monomer bound to RSRSTSTP (see Table S11). In both cases Pro261 formed contacts with Ser46 and Val47 of the protein (see Table S6). These interactions likely exist due to the negatively charged C-terminus placed at Pro261 (for RSRSTSTP/RSRSTpSTP) or Pro9 (for RLYHSLP/RLYHpSLP) in the simulated peptides. This could be an artifact of simulating only a short peptide instead of a long one, which would place its C-terminus outside of the binding groove. This could also be the reason why we observed nearly no unbinding of the unphosphorylated peptides in our simulations even though their binding affinity to 14-3-3 proteins is too weak to be measured in experiment.[9,16,17] Thus the binding affinity of the unphosphorylated peptides is likely altered and possibly overestimated in our alchemical simulations of 14-3-3η monomers with the RSRSTSTP/RSRSTpSTP and RLYHSLP/RLYHpSLP peptides shown below. Previously it was argued that a proline at position +2 from the phosphoserine opens up the possibility for the peptide chain to make a turn in order to be able to also bind to the other binding pocket of a 14-3-3 dimer.[9–11]

We also compared the number of hydrogen bonds accepted by the phosphate oxygen atoms of phosphoserine in the bound and free (completely solvated) states (see Table 3). The phosphate of the phosphorylated RSRSTpSTP peptide formed slightly more hydrogen bonds in the bound state than in the free state. This holds true no matter if the OG oxygen from the original serine side chain is taken into account ($\Delta\# = 0.109 \pm 0.017$, $d = 0.08$) or not ($\Delta\# = 0.453 \pm 0.018$, $d = 0.40$), but calculating Cohen's d shows that the former is not a

TABLE 1 Mean C_α-RMSD from starting structures

	Simulation	Mean C_α-RMSD (Å)
14-3-3η monomer	Without peptide	2.952 ± 0.001
	With RSRSTSTP	3.686 ± 0.002
	With RSRSTpSTP	2.909 ± 0.001
	With RLYHSLP	3.355 ± 0.001
	With RLYHpSLP	2.795 ± 0.001
14-3-3η dimer	Without peptides	3.628 ± 0.002
	With RSRSTSTP	3.397 ± 0.002
	With RSRSTpSTP	3.794 ± 0.002
	With RSRSTSTP + HRYSTP	3.995 ± 0.002
	With RSRSTSTP + HRYpSTP	3.566 ± 0.002
	With RSRSTpSTP + HRYSTP	4.127 ± 0.003
	With RSRSTpSTP + HRYpSTP	3.490 ± 0.001

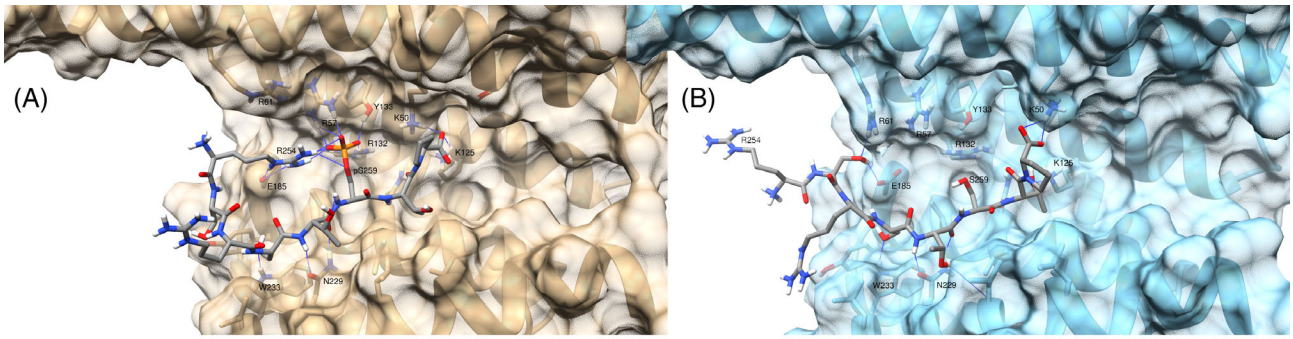

FIGURE 2 Representative structures of a phosphorylated RSRSTpSTP (doubly charged, SP2; left hand side) and an unphosphorylated RSRSTSTP peptide (right hand side) bound to 14-3-3η obtained by a centroid search of all trajectory frames. Pairwise RMSD was computed as a distance metric and the pairwise distances were then used to calculate a pairwise similarity. The centroid is the frame with the highest sum of similarities

TABLE 2 Residue contacts between a 14-3-3η monomer and RSRSTpSTP/RSRSTSTP peptides and respective mean interaction energies

RSRSTpSTP (31 contacts)		
Residue pair	**Distance [Å]**	**Int. energy [kJ/mol]**
ARG57–SP2259	1.7	−512.26
ARG132–SP2259	1.66	−488.15
LYS50–PRO261	2.26	−250.97
LYS125–PRO261	3.14	−250.01
LYS50–SP2259	3.5	−240.85
GLU185–ARG254	3.3	−233.96
TYR133–SP2259	1.7	−120.62
LYS125–THR260	2.49	−48.92
ASN178–THR260	1.93	−40.68
LYS50–THR260	3.74	−30.07
ASN229–THR258	2.09	−26.34
ASN178–SP2259	2.58	−25.64
ASN229–SER257	2.64	−19.68
VAL181–SP2259	2.5	−18.23
TRP233–SER257	2.57	−14.28
LEU232–ARG256	2.77	−7.32
LEU225–SP2259	3.42	−5.66
LEU225–THR258	2.44	−5.23
GLY174–THR260	2.36	−5.19
ILE222–THR260	2.57	−4.89
LEU177–SP2259	2.86	−4.83
GLU185–SER257	3.73	−4.8
LEU177–THR260	2.33	−3.59
TYR184–SER257	2.84	−3.56
VAL181–THR258	3.35	−3.08
LEU177–THR258	2.93	−2.49
VAL181–SER257	3.11	−2.46
LEU225–THR260	2.76	−0.88
LEU232–SER257	2.71	−0.79
ARG132–ARG254	3.9	0.0
ARG57–ARG254	3.34	123.28
LYS50–PRO261	2.07	−239.55
LYS125–PRO261	3.21	−211.84
LYS125–THR260	2.39	−56.84
ASN178–THR260	2.47	−23.84
ASN178–SER259	2.71	−18.34
ARG132–SER259	3.96	−13.34
LEU225–THR258	3.94	−5.74
LEU177–SER259	2.56	−3.48
LEU177–THR260	3.17	−3.19
ILE222–THR260	3.93	−2.41
LEU177–THR258	3.51	−2.11
GLY174–THR260	3.71	−1.47
VAL181–SER259	3.56	−1.17

Note: Here, all contacts were counted if the mean of the shortest atom distance (in Å) between two residues over all frames of three repeated simulations was below 4 Å. The first residue belongs to the protein and the second one to the peptide. SP2259 denotes the phosphorylated (doubly charged) SER259.

relevant difference whereas the latter one is. If only the hydrogen bonds involving the oxygen atoms and the protein or water are considered, instead of also including intrapeptide hydrogen bonds, the effect is even more pronounced ($\Delta\# = 1.406 \pm 0.019$, $d = 0.96$ with OG and $\Delta\# = 1.906 \pm 0.015$, $d = 1.41$ without OG). Thus, the phosphate is energetically better coordinated in the bound state than in the free state. Also, three of the four very close contacts (<2 Å) between the protein and the RSRSTpSTP peptide are formed as strong salt bridges between a charged protein residue and the phosphoserine.

For the unphosphorylated RSRSTSTP peptide one can only analyze the OG atom of the serine side chain. Its coordination in the free state is clearly stronger than in the bound state. Also, its hydrogen-bonding pattern shows more variability (highest occupancy is around 87%) than for the phosphorylated peptide where multiple hydrogen bonds involving mostly phosphoserine exist for close to 100% of the time (see Table 4). The same holds true for the 14-3-3η dimer binding a single RSRSTSTP/RSRSTpSTP peptide (see Table S3). The representative snapshot of the bound RSRSTSTP peptide in Figure 2 also supports these findings. In that figure, the serine side chain is trying to orient toward the surrounding water instead of binding to a 14-3-3η residue. The same also applies to the 14-3-3η dimer binding the RSRSTSTP and RSRSTpSTP peptides (see Tables S3 to S5). Interestingly, the interaction between Asp178 of the protein and the backbone of peptide residue Thr260 is much tighter and more stable when the phosphorylated peptide rather than the unphosphorylated RSRSTSTP peptide is bound either to the 14-3-3η monomer (see Tables 2 and 4) or to the 14-3-3η dimer (compare Tables S3 and S6). The stronger contacts formed by phosphorylated peptides are thus not only due to the direct interactions of the phosphate with charged protein residues but also involve further hydrogen bonds/contacts.

When the 14-3-3η monomer is instead bound to the RLYHSLP and RLYHpSLP peptides, one observes a very similar coordination of the phosphate group in the bound and free states (the effect is much stronger here, see Table S1). Yet the hydrogen bonds are more variable for the phosphorylated RLYHpSLP peptide than for the motif 1 peptide RSRSTpSTP (see Table S2). A particularly noteworthy interaction is that between Asp229 of the 14-3-3η monomer and His6 of the peptide, which is at position +1 from the serine/phosphoserine. This tight interaction seems to pull the entire peptide chain away from the basic pocket that usually accommodates the phosphate group, as well as the side chain of the serine. This effect explains the reduced hydrogen-bond occupancy of the phosphate group but could also further reduce the binding affinity of the unphosphorylated peptide, because all interactions with the binding pocket are reduced in favor of this single interaction.

Next we investigated the contacts between peptide residues next to phosphoserine and protein residues. Interestingly, such contacts mostly involved backbone atoms of these peptide residues (except for His6 in the RLYHSLP/RLYHpSLP peptides). This matches the experimental findings that motif 1 and 2 peptides do not have preferred amino acids at positions −1 and +1 next to the phosphorylated residue.

TABLE 3 Mean number (#) of hydrogen bonds of each oxygen atom in the serine/phosphoserine side chains of the RSRSTSTP/RSRSTpSTP peptides in the bound (monomer simulation) and free state

RSRSTSTP				
	H_2O + protein + peptide		H_2O + protein	
Atom	Bound	Free	Bound	Free
OG	0.395 ± 0.002 (SD: 0.547)	0.740 ± 0.002 (SD: 0.640)	0.240 ± 0.002 (SD: 0.451)	0.740 ± 0.002 (SD: 0.640)
OE1	3.580 ± 0.003 (SD: 0.576)	3.426 ± 0.003 (SD: 0.770)	2.539 ± 0.003 (SD: 0.692)	1.881 ± 0.004 (SD: 0.992)
OE2	3.122 ± 0.002 (SD: 0.346)	3.402 ± 0.003 (SD: 0.730)	3.122 ± 0.002 (SD: 0.346)	1.826 ± 0.004 (SD: 1.039)
OE	4.041 ± 0.003 (SD: 0.674)	3.461 ± 0.003 (SD: 0.735)	3.413 ± 0.003 (SD: 0.676)	3.461 ± 0.003 (SD: 0.735)
Total (no OG)	10.743 ± 0.006 (SD: 0.952)	10.289 ± 0.008 (SD: 1.294)	9.074 ± 0.006 (SD: 1.027)	7.168 ± 0.009 (SD: 1.613)
Total	11.137 ± 0.008 (SD: 1.098)	11.029 ± 0.010 (SD: 1.444)	9.314 ± 0.007 (SD: 1.122)	7.907 ± 0.011 (SD: 1.736)
RSRSTSTP				
	H_2O + protein + peptide		H_2O + protein	
Atom	Bound	Free	Bound	Free
OG	0.978 ± 0.003 (SD: 0.627)	1.191 ± 0.002 (SD: 0.623)	0.975 ± 0.003 (SD: 0.628)	1.173 ± 0.002 (SD: 0.629)

Note: Columns two and three termed H_2O + protein + peptide (free: H_2O + peptide) list the counts of hydrogen bonds between the oxygen atoms of (phospho)serine listed in the first column from the left and atoms from the surrounding water, the protein, and the rest of the peptide (free: water and peptide). Columns four and five labeled H_2O + protein (free: H_2O) contain the counts of hydrogen bonds without the ones connecting the oxygen atoms to the peptide itself.

In the simulation of the 14-3-3η monomer with phosphorylated RSRSTpSTP peptide and the one of the dimer with the same peptide we noticed interactions between Arg254 and Arg256 of the peptide and the phosphate group of pSer259 (combined in around 58% of frames). Similar interactions were formed between Arg3 and the phosphate of pSer7 in the simulations of a 14-3-3η monomer with the phosphorylated RLYHSLP peptide (in around 78% of frames). These interactions led to a nearly completely closed positively charged pocket that shields the phosphoserine from the water and leads to an even better coordination of the phosphate oxygen atoms. No such interaction with the respective serine side chain was found in simulations where an unphosphorylated peptide was bound to 14-3-3η.

In order to study how peptide binding affects the stability of the 14-3-3η monomer we then performed an RMSF analysis of the trajectories. Figure 4 shows that the binding of peptides did not notably influence the fluctuations of the 14-3-3η monomer. A small difference can be seen for residues 166 to 233 when binding the phosphorylated RSRSTpSTP peptide (blue curve) whereas for the monomer binding the same peptide in a dimer simulation with a single peptide (not shown) only residues 204 to 233 showed slightly reduced fluctuations. The second monomer in the dimer simulation showed no differences between binding no peptide, RSRSTSTP, or RSRSTpSTP, respectively. For the 14-3-3η monomer binding either the RLYHSLP or the RLYHpSLP peptides no differences were found when compared with each other or to the monomer without peptides. The 14-3-3η dimer bound to two peptides also showed hardly any difference no matter if both peptides were phosphorylated, unphosphorylated, or mixed.

3.2 | Principal component analysis

Next we wanted to find out if the binding of the peptides has an influence on the internal low-frequency modes of the 14-3-3η dimer. For this we performed a principal component analysis (PCA) analysis on the three concatenated simulations of each system. As baseline we used the main modes of the 14-3-3η dimer without bound peptides. As expected, the first mode is an opening-closing movement of the two monomers toward each other without twisting, where the tips of the monomers (at the opposite ends of the dimer interface) move closer to each other when closing and away from each other when opening. The movement of the monomer tips is quite pronounced ($\approx$15 Å for each tip). Similar first modes were obtained when the dimer is bound at the same time to the RSRSTpSTP and HRYpSTP peptides or to the RSRSTSTP and HRYSTP peptides. All other cases include strong twisting in their first modes.

TABLE 4 Percent hydrogen-bond occupancies for hydrogen bonds between 14-3-3η monomers and RSRSTSTP/RSRSTpSTP peptides, which exist in more than 10% of all simulation frames

RSRSTpSTP (26 pairs)	
Residue pair	**Occupancy (%)**
TYR133-OH–SP2259-OE2	99.99
ARG132-NH1–SP2259-OE1	99.91
ARG132-NH2–SP2259-OE2	99.17
ASN178-OD1–THR260-N	98.23
ARG57-NH2–SP2259-OE1	97.31
ARG57-NH1–SP2259-OE	96.11
ASN229-ND2–THR258-O	83.71
ASN178-ND2–THR260-O	66.00
ASN229-OD1–THR258-N	48.12
TRP233-NE1–SER257-OG	39.83
LYS50-NZ–PRO261-OXT	39.25
LYS50-NZ–PRO261-O	37.74
LYS125-NZ–PRO261-OXT	37.24
LYS125-NZ–PRO261-O	34.88
ARG57-NH1–SP2259-OE1	34.41
GLU185-OE1–ARG254-NH2	31.68
GLU185-OE2–ARG254-NH2	31.09
LYS125-NZ–THR260-OG1	29.84
LYS125-NZ–THR260-O	28.53
ASN178-OD1–THR260-OG1	27.03
ARG132-NH1–SP2259-OE2	26.80
GLU185-OE2–ARG254-NE	23.47
GLU185-OE1–ARG254-NE	21.38
LYS50-NZ–SP2259-OE	18.23
ASN178-ND2–THR260-OG1	15.58
ASN229-OD1–SER257-OG	11.10
ASN229-ND2–THR258-O	86.86
ASN229-OD1–THR258-N	75.79
ASN178-OD1–THR260-N	74.06
LYS50-NZ–PRO261-OXT	69.97
LYS50-NZ–PRO261-O	66.16
TRP233-NE1–SER257-OG	43.83
LYS125-NZ–THR260-OG1	39.35
ASN178-ND2–THR260-O	38.32
ASN178-ND2–THR260-OG1	37.01
GLU185-OE1–SER255-OG	28.99
ARG132-NH1–SER259-OG	28.19
LYS125-NZ–PRO261-O	24.68
GLU185-OE2–SER255-OG	23.05
GLU185-OE2–SER257-OG	20.75
GLU185-OE2–SER257-N	20.63
LYS125-NZ–PRO261-OXT	17.08
GLU185-OE2–ARG256-N	16.44
GLU185-OE1–SER257-OG	13.80
GLU185-OE1–SER257-N	13.53
LYS125-NZ–THR260-O	13.08

Note: The first residue belongs to the protein and the second one to the peptide.

The second PCA mode is a twisting movement of the two monomers that is coupled to a small opening-closing movement. The opening happens when the monomers twist left, the closing when the monomers twist right. Similar second modes are found in all other dimer simulations no matter which peptides are bound. The third PCA mode is an alternating opening and closing of the two monomers where one monomer is open while the other one is closed. Similar third modes were found when the RSRSTpSTP and HRYpSTP peptides or the RSRSTSTP and HRYSTP peptides simultaneously bind to the dimer, when the dimer binds to a single RSRSTSTP peptide and when the RSRSTSTP and HRYpSTP peptides simultaneously bind to the dimer, though in these cases some twisting movement can be seen as well. The third PCA modes of all other simulations differ from this one and likewise from each other.

Overall the principal components of the 14-3-3η dimer with the peptides either both in the phosphorylated or both in the unphosphosporylated state resemble most strongly the ones of the dimer without peptides. The main principal components for dimers bound to a single peptide or when bound to two peptides with differing phosphorylation state differ strongly from the other cases. This shows that the binding of peptides has a strong influence on the dynamics of the full dimer.

3.3 | Alchemical free energy simulations

The results of the unbiased MD simulations suggest that the phosphorylated peptides are much more tightly coordinated in the 14-3-3 binding groove than the unphosphorylated peptides. Additionally, the phosphates were better coordinated inside the binding pocket than in bulk water. On the other hand, the side-chain oxygen atoms of the serines in the unphosphorylated peptides were better coordinated in the free state compared with the bound state. Hence, we set out to quantify the binding free energy differences between the phosphorylated and unphosphorylated forms of three peptides bound to the 14-3-3η monomer with the alchemical transformation method. We analyzed three transformations of the RSRSTSTP to the RSRSTpSTP peptide, of the RSRSTSTPNV to the RSRSTpSTPNV peptide, and of the RLYHSLP to the RLYHpSLP peptide, respectively. All transformations were also performed in the backward direction in order to obtain improved convergence.

At physiological pH = 7.2, the phosphate group exists predominantly in the dibasic form ($-OPO_3^{-2}$, further called SP2) and not in the

TABLE 5 Binding free energy differences in kJ/mol between phosphorylated/unphosphorylated peptides binding to the 14-3-3η domain obtained by alchemical transformations in comparison with experiment at 298.15 K

	Exp. ΔG_{bind}		$\Delta\Delta G_{bind}$		
Peptide	**S**	**pS**	**Exp.**	**Alch. Sim. (SP1)**	**Alch. Sim. (SP2)**
RSRSTpSTP	> -24.55[a]	-35.92[a]	< -11.37	-14.84 ± 5.27	-41.32 ± 6.42
RSRSTpSTPNV					-39.11 ± 4.14
RLYHpSLP		-42.39[b]			-50.80 ± 7.32

[a]Values were calculated from experimental K_I values.
[b]Values were calculated from experimental K_D values by Yaffe et al.[9]

monobasic form ($-OHPO_2^{-2}$, further called SP1) (phosphoserine $pK_a = 5.6$[52]). Therefore, we used the dibasic form in most of our simulations but tested also the monobasic form for the RSRSTSTP to RSRSTpSTP transformation.

The results are listed in Table 5. The experimental value for the absolute binding free energy of the unphosphorylated RSRSTSTP peptide represents a lower margin to the real binding free energy, since the value could not be precisely determined in the experimental assay.[9] Therefore, it is likely much less negative and the binding is therefore much weaker than the binding of the phosphorylated RSRSTpSTP peptide. To our knowledge there exist no experimental binding free energies or binding constants for unphosphorylated motif I, II, and III peptides.[16,53] The only available binding data for unphosphorylated peptides binding to 14-3-3 proteins exist for a range of peptides whose sequences are unrelated to the known 14-3-3 binding motifs.[6,13] Thus, one can expect that the binding free energy for the unphosphorylated peptides studied here is close to zero. The lower experimental limit of the equilibrium binding constant is 50 μmol (for RSRSTSTP binding 14-3-3η)[9] resulting in a minimum binding free energy of -24.55 kJ/mol.

All binding free energy differences reported in this study are defined as the binding free energy of the phosphorylated peptide minus the one of the unphosphorylated peptide $\Delta\Delta G_{bind} = \Delta G_{bind}^{phosphorylated} - \Delta G_{bind}^{unphosphorylated}$. We will discuss the implications of the reported values in the discussion section.

4 | DISCUSSION

The aim of this work was to find out mechanistically why the phosphorylated forms of 14-3-3 binding peptides bind more strongly to 14-3-3 domains than their unphosphorylated counterparts. We selected several systems for which thermodynamic and structural data are available. Thus, we simulated the 14-3-3η monomer complexed with the RSRSTSTP/RSRSTpSTP and RLHYSLP/RLYHpSLP peptides. Additionally we studied the 14-3-3η dimer binding to a single RSRSTSTP/RSRSTpSTP peptide and the dimer binding two peptides at the same time (RSRSTSTP + HRYSTP, RSRSTSTP + HRYpSTP, RSRSTpSTP + HRYSTP, and RSRSTpSTP + HRYpSTP). Our results suggest that there exist (if at all) only small differences between a single peptide binding to a 14-3-3η monomer or to a dimer in terms of the coordination of the phosphate oxygens, the hydrogen bonds, and the contacts between the peptide and the protein, no matter whether the peptide is phosphorylated or not. However, the simulations provide a clear picture why the complex between the 14-3-3η domain (no matter if as monomer or dimer) and the phosphorylated RSRSTpSTP peptide is much more favorable than with the unphosphorylated RSRSTSTP peptide. The main reasons for this are the strong interactions of the phosphate group with charged residues of the 14-3-3η domain, the strengthening of additional hydrogen bonds due to close peptide–protein contacts of the phosphorylated RSRSTpSTP peptide, and the better coordination of the phosphoserine side chain, as well as the weaker coordination of the serine side chain in the bound state compared with the free state. Similar arguments apply to the case when either a phosphorylated RLYHpSLP peptide or an unphosphorylated RLYHSLP peptide (motif 2) binds to a 14-3-3η monomer. We also observed contacts between the arginines at positions -3, -4 and -5 next to the phosphoserine and the phosphate group that likely enhance its coordination in the bound state. This would explain why the most common binding motifs almost always contain arginine residues at positions -3 (motif 1) and -4 (motif 2).[9–11] The same effect will likely also exist for motif 3 peptides that also usually contain an arginine at position -3 from the phosphoserine/phosphothreonine.[10]

We performed simulations of all systems three times over 1 μs each. As can be seen from the hydrogen-bonding patterns (compare Figure 3 and Figures S3–S6) there exist certain differences between replicate simulations. Even hydrogen bonds that include atoms from the phosphoserine residue vary to some extent. Overall this suggests that 1 μs long simulations are too short to sample all important dynamics of the systems. By integrating the results from three independent simulations, we suggest that our findings are an approximation to the real system properties. This is even more relevant for the simulations of the 14-3-3η dimers, since for these many more interactions and also additional dimer movements seem to play a role in the system dynamics.

The binding free energy differences computed using the alchemical free energy transformation method are more negative than the experimental binding free energies for the phosphorylated peptides. Even if the unphosphorylated peptides had absolute binding free energies of zero (so no binding at all, which could be expected since these were too small to be measured experimentally[9,16,17]), the binding free energy difference could not be more negative than the absolute values for the phosphorylated peptides. If the binding free energies of the unphosphorylated peptides are indeed close to zero, the absolute free energies of the phosphorylated peptides would lie in

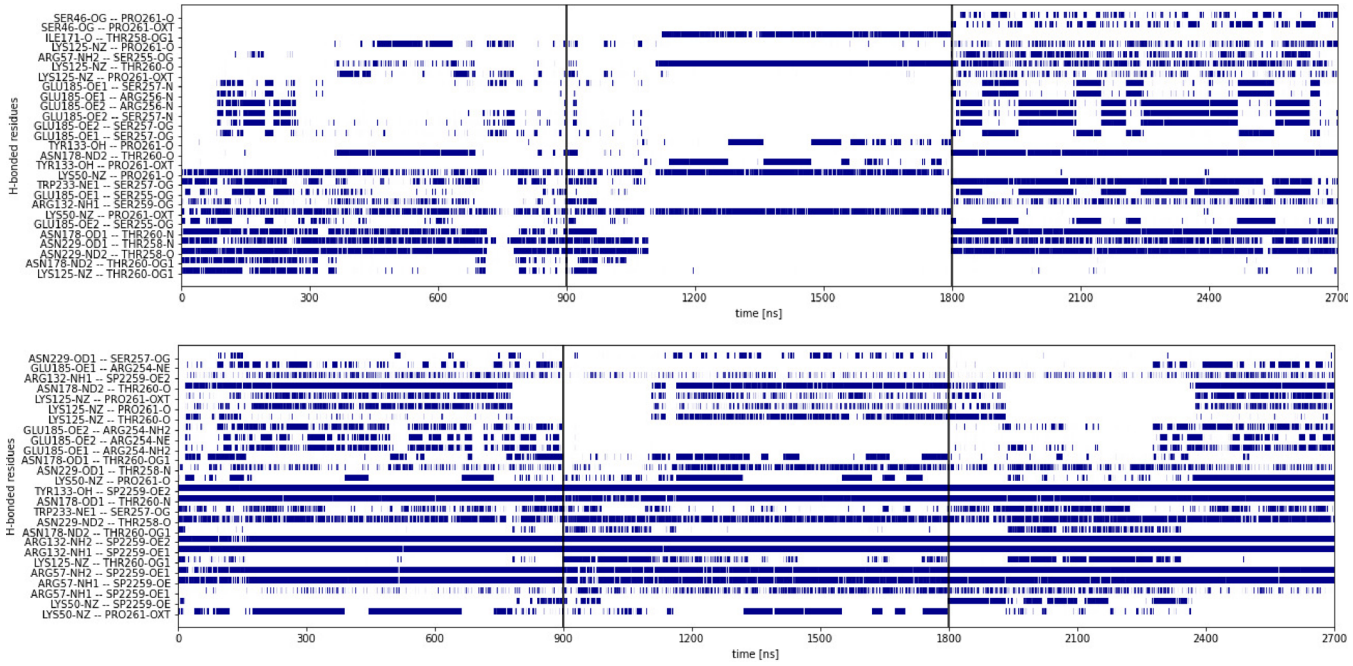

FIGURE 3 Hydrogen bonds present in more than 10% of all frames (white = no hydrogen bond, blue = hydrogen bond) between a 14-3-3η monomer and the RSRSTSTP (top) and RSRSTpSTP (bottom) peptides in a monomer simulation

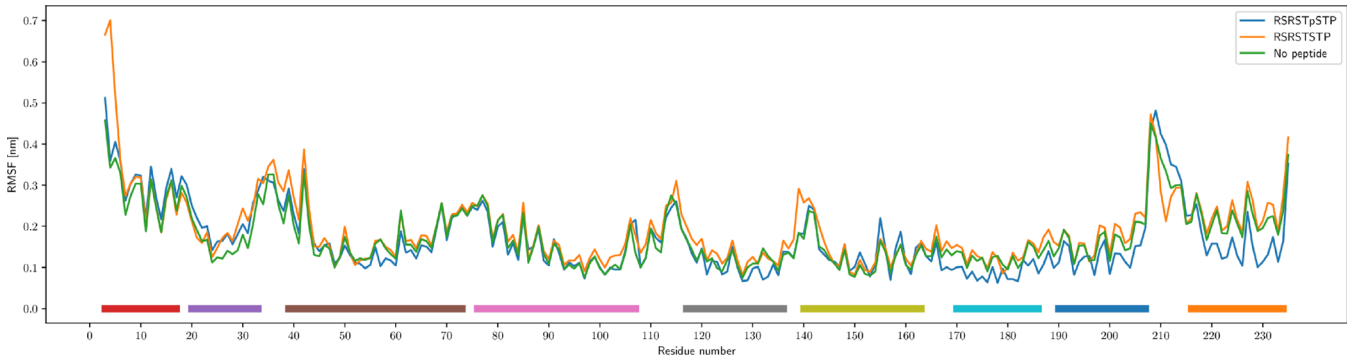

FIGURE 4 Root mean square fluctuations (RMSFs) of the residues in the free 14-3-3η monomer and when bound to the RSRSTSTP and RSRSTpSTP peptides. The helices of the monomer are indicated as colored bars at the bottom of the plot

the error range of the results from the alchemical simulations we report here. Reassuringly, the difference computed for the comparison of RSRSTpSTP/RSRSTSTP and RLYHpSLP/RLYHSLP transformations (9.48 kJ/mol) compares well to the difference of the experimental absolute free energies of the RSRSTpSTP and RLYHpSLP peptides (6.47 kJ/mol). Possibly, the interactions with the phosphate group are slightly overestimated in the CHARMM36m force field.[27]

Cooperative effects among the two binding sites of 14-3-3 dimers have been suggested based on experimental observations.[9,17,19] We tried to analyze if this cooperativity results from entropic effects of the peptide chain or if it stems from some interactions inside the 14-3-3 dimer. However, no particular differences were observed in the contacts between the peptides and the 14-3-3η monomers in simulations of 14-3-3η dimers with two bound peptides at the same time. When the first bound peptide was the phosphorylated RSRSTpSTP, it did not matter if there was a second peptide and what phosphorylation status the second peptide had. The same result was found for HRYpSTP as the first peptide. Hence, this specific result does not support a model where intradimer interactions give rise to cooperativity.

A hint at explaining the cooperativity between the binding of two peptides in addition to entropic effects of the peptide could be the following observation: The results from the principal component analysis of the various 14-3-3η dimer simulations show a substantial influence of the peptide binding on the low frequency modes of the dimer. The binding of a single peptide, no matter if phosphorylated or not, as well as of two peptides with different phosphorylation states alters

dimer dynamics compared with what is observed when no peptide is bound. Instead, when two peptides with the same phosphorylation state are bound, then the normal dimer dynamics were observed. Thus, the internal conformational dynamics of the dimer are left unchanged. This could explain to some extent why it is favorable for the 14-3-3η dimer to bind two phosphorylated peptides at the same time and therefore the cooperativity of the binding.

In summary, we found that studying complexes of 14-3-3 domains with phosphorylated versus non-phosphorylated peptides by means of molecular dynamics simulations is quite challenging. One microsecond simulations appear not fully converged in terms of conformational dynamics, since repeated simulations show slightly different binding behavior of the peptides. Alchemical free energy calculations involving doubly charged groups such as phosphate remain challenging even if one applies tricks such as including a mirror peptide where the perturbation is performed in the opposite direction or corrections for electrostatic effects. Nonetheless, a clear picture emerged from our simulations whereby the 14-3-3 binding groove provides a unique superior coordination for phosphorylated peptides compared with their non-modified counterparts highlighting biomolecular recognition.

ACKNOWLEDGMENT

This project was supported by Deutsche Forschungsgemeinschaft grant He3875/14-1 and Universitaet des Saarlandes (Projekt DEAL).

Molecular graphics and analyses were performed with UCSF Chimera,[22] developed by the Resource for Biocomputing, Visualization, and Informatics at the University of California, San Francisco, with support from NIH P41-GM103311.

Special thanks go to Dr. V. Gapsys from MPI for biophysical chemistry in Goettingen for providing hybrid structures for phosphorylated serines for the CHARMM36m force field to be used in the PMX[25,26] program. Open Access funding enabled and organized by Projekt DEAL.

PEER REVIEW

The peer review history for this article is available at https://publons.com/publon/10.1002/prot.26224.

DATA AVAILABILITY STATEMENT

The data that support the findings of this study are available from the corresponding author upon reasonable request.

ORCID

Volkhard Helms https://orcid.org/0000-0002-2180-9154

REFERENCES

1. Aitken A. 14-3-3 and its possible role in co-ordinating multiple signalling pathways. *Trends Cell Biol*. 1996;6:341-347.
2. Fu H, Subramanian RR, Masters SC. 14-3-3 proteins: structure, function, and regulation. *Annu Rev Pharmacol Toxicol*. 2000;40:617-647.
3. Woodcock JM, Goodwin KL, Sandow JJ, et al. Role of salt bridges in the dimer interface of 14-3-3ζ in dimer dynamics, N-terminal α-helical order, and molecular chaperone activity. *J Biol Chem*. 2018;293:89-99.
4. Bridges D, Moorhead GBG. 14-3-3 proteins: a number of functions for a numbered protein. *Sci STKE*. 2005;2005:re10-re10.
5. Gardino AK, Smerdon SJ, Yaffe MB. Structural determinants of 14-3-3 binding specificities and regulation of subcellular localization of 14-3-3-ligand complexes: a comparison of the X-ray crystal structures of all human 14-3-3 isoforms. *Semin Cancer Biol*. 2006;16(3):173-182.
6. Petosa C, Masters SC, Bankston LA, et al. 14-3-3ζ binds a phosphorylated Raf peptide and an unphosphorylated peptide via its conserved amphiphatic groove. *J Biol Chem*. 1998;273:16305-16310.
7. Zhang L, Wang H, Liu D, Liddington R, Fu H. Raf-1 kinase and exoenzyme S interact with 14-3-3ζ through a common site involving lysine 49. *J Biol Chem*. 1997;272:13717-13724.
8. Wang H, Zhang L, Liddington R, Fu H. Mutations in the hydrophobic surface of an amphiphatic groove of 14-3-3ζ disrupt its interaction with Raf-1 kinase. *J Biol Chem*. 1998;273:16297-16304.
9. Yaffe MB, Rittinger K, Volinia S, et al. The structural basis for 14-3-3: phosphopeptide binding specificity. *Cell*. 1997;91:961-971.
10. Ganguly S, Weller JL, Ho A, Chemineau P, Malpaux B, Klein DC. Melatonin synthesis: 14-3-3-dependent activation and inhibition of arylalkylamine N-acetyltransferase mediated by phosphoserine-205. *Proc Natl Acad Sci U S A*. 2005;102:1222-1227.
11. Tugaeva KV, Kalacheva DI, Cooley RB, Strelkov SV, Sluchanko NN. Concatenation of 14-3-3 with partner phosphoproteins as a tool to study their interaction. *Sci Rep*. 2019;9:15007.
12. Aitken A. 14-3-3 proteins: a historic overview. *Semin Cancer Biol*. 2006;16:162-172.
13. Ottmann C, Yasmin L, Weyand M, et al. Phosphorylation-independent interaction between 14-3-3 and exoenzyme S: from structure to pathogenesis. *EMBO J*. 2007;26:902-913.
14. Sato S, Jung H, Nakagawa T, et al. Metabolite regulation of nuclear localization of carbohydrate-response element-binding protein (ChREBP): role of AMP as an allosteric inhibitor*. *J Biol Chem*. 2016;291:10515-10527.
15. Sijbesma E, Visser E, Plitzko K, et al. Structure-based evolution of a promiscuous inhibitor to a selective stabilizer of protein-protein interactions. *Nat Commun*. 2020;11:3954-3954.
16. Muslin AJ, Tanner JW, Allen PM, Shaw AS. Interaction of 14-3-3 with signaling proteins is mediated by the recognition of phosphoserine. *Cell*. 1996;84:889-897.
17. Kostelecky B, Saurin AT, Purkiss A, Parker PJ, McDonald NQ. Recognition of an intra-chain tandem 14-3-3 binding site within PKCe. *EMBO Rep*. 2009;10:983-989.
18. Yaffe MB. How do 14-3-3 proteins work? - gatekeeper phosphorylation and the molecular anvil hypothesis. *FEBS Lett*. 2002;513:53-57.
19. Molzan M, Ottmann C. Synergistic binding of the phosphorylated S233- and S259-binding sites of C-RAF to one 14-3-3ζ dimer. *J Mol Biol*. 2012;423:486-495.
20. Berman HM, Westbrook J, Feng Z, et al. The protein data bank. *Nucleic Acids Res*. 2000;28:235-242.
21. Yang X, Lee WH, Sobott F, et al. Structural basis for protein–protein interactions in the 14-3-3 protein family. *Proc Natl Acad Sci*. 2006;103:17237-17242.
22. Pettersen EF, Goddard TD, Huang CC, et al. UCSF chimera—a visualization system for exploratory research and analysis. *J Comput Chem*. 2004;25:1605-1612.
23. Rittinger K, Budman J, Xu J, et al. Structural analysis of 14-3-3 phosphopeptide complexes identifies a dual role for the nuclear export signal of 14-3-3 in ligand binding. *Mol Cell*. 1999;4:153-166.
24. Dunbrack RL. Rotamer libraries in the 21st century. *Curr Opin Struct Biol*. 2002;12:431-440.
25. Gapsys V, Michielssens S, Seeliger D, de Groot BL. pmx: automated protein structure and topology generation for alchemical perturbations. *J Comput Chem*. 2015;36:348-354.
26. Gapsys V, de Groot BL. pmx webserver: a user friendly interface for alchemistry. *J Chem Inf Model*. 2017;57:109-114.

27. Huang J, Rauscher S, Nawrocki G, et al. CHARMM36m: an improved force field for folded and intrinsically disordered proteins. *Nat Methods*. 2016;14:71-73.
28. Abraham MJ, Murtola T, Schulz R, et al. GROMACS: high performance molecular simulations through multi-level parallelism from laptops to supercomputers. *SoftwareX*. 2015;1-2:19-25.
29. Jorgensen WL, Chandrasekhar J, Madura JD, Impey RW, Klein ML. Comparison of simple potential functions for simulating liquid water. *J Chem Phys*. 1983;79:926-935.
30. MacKerell AD, Bashford D, Bellott M, et al. All-atom empirical potential for molecular modeling and dynamics studies of proteins. *J Phys Chem B*. 1998;102:3586-3616.
31. Makov G, Payne MC. Periodic boundary conditions in ab initio calculations. *Phys Rev B*. 1995;51:4014-4022.
32. Essmann U, Perera L, Berkowitz ML, Darden T, Lee H, Pedersen LG. A smooth particle mesh Ewald method. *J Chem Phys*. 1995;103:8577-8593.
33. Hess B, Bekker H, Berendsen HJC, Fraaije JGEM. LINCS: a linear constraint solver for molecular simulations. *J Comput Chem*. 1997;18:1463-1472.
34. Bussi G, Donadio D, Parrinello M. Canonical sampling through velocity rescaling. *J Chem Phys*. 2007;126:014101.
35. Berendsen HJC, Postma JPM, van Gunsteren WF, DiNola A, Haak JR. Molecular dynamics with coupling to an external bath. *J Chem Phys*. 1984;81:3684-3690.
36. Parrinello M, Rahman A. Polymorphic transitions in single crystals: a new molecular dynamics method. *J Appl Phys*. 1981;52:7182-7190.
37. Nosé S, Klein M. Constant pressure molecular dynamics for molecular systems. *Mol Phys*. 1983;50:1055-1076.
38. McGibbon RT, Beauchamp KA, Harrigan MP, et al. MDTraj: a modern open library for the analysis of molecular dynamics trajectories. *Biophys J*. 2015;109:1528-1532.
39. Baker E, Hubbard R. Hydrogen bonding in globular proteins. *Prog Biophys Mol Biol*. 1984;44:97-179.
40. Jarzynski C. Nonequilibrium equality for free energy differences. *Phys Rev Lett*. 1997;78:2690-2693.
41. Bennett CH. Efficient estimation of free energy differences from Monte Carlo data. *J Comput Phys*. 1976;22:245-268.
42. Goette M, Grubmüller H. Accuracy and convergence of free energy differences calculated from nonequilibrium switching processes. *J Comput Chem*. 2009;30:447-456.
43. Gilson MK, Given JA, Bush BL, McCammon JA. The statistical-thermodynamic basis for computation of binding affinities: a critical review. *Biophys J*. 1997;72:1047-1069.
44. General IJ. A note on the standard state's binding free energy. *J Chem Theory Comput*. 2010;6:2520-2524.
45. Hünenberger PH, McCammon JA. Ewald artifacts in computer simulations of ionic solvation and ion-ion interaction: a continuum electrostatics study. *J Chem Phys*. 1999;110:1856-1872.
46. Kastenholz MA, Hünenberger PH. Influence of artificial periodicity and ionic strength in molecular dynamics simulations of charged biomolecules employing lattice-sum methods. *J Phys Chem B*. 2004;108:774-788.
47. Kastenholz MA, Hünenberger PH. Computation of methodology-independent ionic solvation free energies from molecular simulations. II. The hydration free energy of the sodium cation. *J Chem Phys*. 2006;124:224501.
48. Reif MM, Hünenberger PH. Computation of methodology-independent single-ion solvation properties from molecular simulations. III. Correction terms for the solvation free energies, enthalpies, entropies, heat capacities, volumes, compressibilities, and expansivities of solvated ions. *J Chem Phys*. 2011;134:144103.
49. Rocklin GJ, Mobley DL, Dill KA, Hünenberger PH. Calculating the binding free energies of charged species based on explicit-solvent simulations employing lattice-sum methods: an accurate correction scheme for electrostatic finite-size effects. *J Chem Phys*. 2013;139:184103.
50. Chen W, Deng Y, Russell E, Wu Y, Abel R, Wang L. Accurate calculation of relative binding free energies between ligands with different net charges. *J Chem Theory Comput*. 2018;14:6346-6358.
51. Xiong H, Crespo A, Marti M, Estrin D, Roitberg AE. Free energy calculations with non-equilibrium methods: applications of the Jarzynski relationship. *Theor Chem Acc*. 2006;116:338-346.
52. Xie Y, Jiang Y, Ben-Amotz D. Detection of amino acid and peptide phosphate protonation using Raman spectroscopy. *Anal Biochem*. 2005;343:223-230.
53. Espejo AB, Gao G, Black K, et al. PRMT5 C-terminal phosphorylation modulates a 14-3-3/PDZ interaction switch. *J Biol Chem*. 2017;292:2255-2265.

SUPPORTING INFORMATION

Additional supporting information may be found in the online version of the article at the publisher's website.

How to cite this article: Künzel N, Helms V. How phosphorylation of peptides affects their interaction with 14-3-3η domains. *Proteins*. 2022;90(2):351-362. doi: 10.1002/prot.26224